Real-space Green's function approach to angle-resolved resonant photoemission: Spin polarization and circular dichroism in itinerant magnets

Fabiana Da Pieve[1,*] and Peter Krüger[2]

[1]*ALGC, Vrije Universiteit Brussel, Pleinlaan 2, Brussels 1050, Belgium*

[2]*Graduate School of Advanced Integration Science, Chiba University, 1-33 Yayoi-cho, Inage, Chiba 263-8522, Japan*

(Received 16 June 2013; published 12 September 2013)

A first-principles approach, based on the real-space multiple scattering Green's function method, is presented for spin- and angle-resolved resonant photoemission from magnetic surfaces. It is applied to the Fe(010) valence band photoemission excited with circularly polarized x rays around the Fe L_3 absorption edge. When the photon energy is swept through the Fe $2p$-$3d$ resonance, the valence band spectra are strongly modified in terms of absolute and relative peak intensities, degree of spin polarization, and light polarization dependence. New peaks in the spin-polarized spectra are identified as spin-flip transitions induced by exchange decay of spin-mixed core holes. By comparison with single-atom and band-structure data, it is shown that both intra-atomic and multiple scattering effects strongly influence the spectra. We show how the different features linked to states of different orbital symmetry in the d band are differently enhanced by the resonant effect. The appearance and origin of circular dichroism and spin polarization are analyzed for different geometries of light incidence and electron emission direction, providing guidelines for future experiments.

DOI: 10.1103/PhysRevB.88.115121 PACS number(s): 78.20.Bh, 78.20.Ls, 78.70.−g, 79.60.−i

In the last decade, magnetic circular dichroism (MCD) and spin-polarization studies in resonant inelastic x-ray scattering (RIXS) and resonant photoemission (RPES) have acquired great importance in the study of magnetic and correlated materials. Such spectroscopies probe, respectively, the radiative and nonradiative autoionization decay of a core hole, and the signal can be strongly enhanced with respect to the nonresonant mode. The element and orbital selectivity of core-level resonant spectroscopies allows us to access higher-order multipoles which are left unexplored by MCD in x-ray absorption (XAS),[1–6] to distinguish and enhance specific electronic excitations and satellites,[7,8] collective magnetic excitations,[9] ultrafast and charge-transfer dynamics,[10–12] and to detect quadrupolar transitions towards localized empty states.[13,14] In particular, RPES has recently been applied to several correlated materials[15–19] and full two-dimensional angular scans of resonantly emitted electrons in moderately correlated materials have also been carried out.[20,21] These works, together with earlier pioneering studies[22,23] on local magnetic properties in macroscopically nonmagnetic systems, demonstrate the importance of RPES and the need for an advancement in the theoretical description of this spectroscopy, which is the main aim of this work.

RPES is in principle an autoionization channel of the more general process called resonant Auger decay. Depending on whether the core-excited electron participates or not in the Auger decay, the process is termed either participator or spectator channel. In the participator channel, the one-hole final state is degenerate with the one in direct valence band photoemission (PES, or ARPES if angle resolved). Thus, the two processes generally interfere, giving rise to a typical Fano profile,[24] and the emission is often strongly enhanced. This autoionization channel shows linear dispersion of the spectral features with photon energy (Raman regime), as direct PES, and it is the one that, strictly speaking, constitutes the RPES. The spectator channel, on the contrary, leads to an Auger-like final state with two holes, and the spectral lines exhibit a normal Auger behavior. However, often the enhancement of the direct valence band PES is given by the combination of the two different photoemissionlike and Auger-like channels[12,15,25–27] and, in order to distinguish between the two regimes, it is in principle necessary to perform measurements with a photon energy bandwidth smaller than the core linewidth.

Exploiting the polarization properties of the light, the angle-resolved and spin-polarized detection of the decay products can allow us in principle to perform highly differential experiments. Several works have been devoted to the study of dichroism in the resonant Auger decay (with focus on the spectator channels), in normal Auger emission, and in RIXS.[3,28–31] The different excitation conditions in the resonant and normal Auger process result in a different degree of polarization for the intermediate core hole (nearly no polarization in normal Auger), consequently leading to a different MCD. The experimental geometry that is often considered is the so-called *transverse* or *perpendicular geometry*, in which the photon beam is perpendicular to the magnetization. In this case, the MCD in absorption vanishes and it has been shown that $2p3p3p$ RPES directly displays the quadrupole moment of the core hole[1] (the $3d$ shell is merely a spectator in such decay). Decay processes involving open shells, such as core-core-valence and core-valence-valence decays, are more complicated and have not been discussed in such previous works, nor have the photoelectron diffraction effects. Furthermore, similarly to direct photoemission/Auger emission from magnetic surfaces, adding spin resolution to the magnetic dichroism analysis can allow us to separate different contributions to the spin polarization (SP) of the outgoing electrons,[32–35] but understanding the interplay between dichroism and spin polarization in autoionization channels is not straightforward.

While several theoretical formulations have recently been proposed for RIXS,[9,36] similar theoretical effort is lacking for RPES. At present, the interpretation of RPES in solids is essentially based on localized models[30,37] supported by

multiplet calculations, with focus mainly on the spectator channel with well-defined two-hole final states. Recently, we have presented a first-principles approach based on real-space multiple scattering (RSMS),[38] with explicit calculations for Cr, a weak antiferromagnet. Such a method represents a practical computational scheme which allows us to consider the band structure of the system, probed by the multiple scattering events felt by the excited electrons.

In this work, we reformulate our approach within a Green's function formalism and we perform calculations for spin- and angle-resolved direct valence band PES (spin-resolved ARPES) and RPES (spin-resolved AR-RPES) for Fe(010) for excitations at the L_3 edge by circularly polarized light. The paper is organized as follows: In Sec. I, we present the theoretical description of the resonant process via a Green's function formalism and we give details about the calculations; in Sec. II A, we discuss single-atom results, allowing for a clear explanation of the resonance mechanism, the discrimination of intra-atomic effects in spin-flip transitions and spin-polarization effects; in Sec. II B, we move to the full cluster results, investigating the enhancement of the peaks in relation to electronic states of different spin and orbital symmetry, the spin-flip transitions, and the multiple scattering effects in different geometrical conditions. Improvements to our approach are also discussed.

I. THEORETICAL FORMULATION

Previous formulations of RPES are due to Davis and Feldkamp[39] in terms of the interaction between discrete and continuum states and by Åberg *et al.*[40,41] in the frame of a unified theory of inelastic scattering with the time-independent scattering theory including asymptotically the double-emission region. RPES was also reviewed by Gel'mukhanov and Ågren.[42] Previous RPES calculations have been carried out with semiempirical methods, using either a band picture[43,44] or a charge-transfer cluster model.[30,37,45]

Here, we will base our formulation on real-space multiple scattering theory, excluding the region of double emission, which was previously treated in a separate work.[46] We will limit ourselves to the participator channel. A strict distinction between such a channel and the spectator one is only meaningful in the single-particle approach, which is justifiable here as we are mainly interested in effects related to the nature of the dichroism itself or effects related to the specific direction of the photoelectron.

The theoretical description and computational method for RPES within RSMS have been described in our previous work on Cr(110).[38] For the convenience of the reader, we shall outline the method here again via a more general Green's function formulation. In the following, $|\cdots)$ and $|\cdots\rangle$ denote many-electron and one-electron states, respectively. Most generally, the photoemission intensity is given by

$$I = \sum_f |(f|T|0)|^2 \delta(\hbar\omega + E_0 - E_F), \tag{1}$$

where $\hbar\omega$ is the photon energy, $|0)$ the electronic ground state with energy E_0, and $|f)$ a final state with an electron in the continuum state $|k\rangle$ and a hole in a valence state $|v\rangle$. T denotes the transition operator. In the independent particle approximation (IPA), the final states are of the form $|f) = a_k^+ a_v|0)$ where a, a^+ denote annihilation and creation operators. Using the IPA and a one-step model, Pendry[47] showed that the (nonresonant) photocurrent can be written as

$$I = -\frac{1}{\pi}\mathrm{Im}\langle\phi|G^+(\epsilon_k)TG^+(\epsilon_v)T^+G^-(\epsilon_k)|\phi\rangle. \tag{2}$$

Here, ϕ is a plane wave with energy ϵ_k as observed at the electron detector. This wave is propagated into the crystal by the advanced single-particle Green's function $G^-(\epsilon_k)$, such that the total photoelectron final state $|k\rangle \equiv G^-(\epsilon_k)|\phi\rangle$ is a time-reversed low-energy electron diffraction (LEED) state. $G^+(\epsilon_v)$ is the retarded Green's function which describes propagation of the electron inside the crystal with initial state energy $\epsilon_v = \epsilon_k - \hbar\omega$. In nonresonant conditions, T is given by the optical (dipole) operator D. Electron correlation and lifetime effects may be accounted for in a quasiparticle picture by introducing a complex self-energy in the calculation of $G^+(\epsilon_v)$ and $G^-(\epsilon_k)$.[48]

For photon energies ω around an x-ray absorption threshold, a second transition channel opens up which leads to the same PE final state $|f) = a_k^+ a_v|0)$ as normal photoemission. This resonant channel consists of a virtual x-ray absorption process followed by an autoionization (or "participator Auger") decay. To lowest order in the autoionization operator V, the transition operator T then becomes[45,49,50]

$$T(\omega) = D + \sum_m \frac{V|m)(m|D}{\omega + E_0 - E_m - i\Gamma_m}. \tag{3}$$

The sum runs over all intermediate states $|m)$ with energy E_m and lifetime width Γ_m. Here, the relevant states $|m)$ are core-excited absorption final states. In the IPA they are of the form $a_u^+ a_c|0)$, where $|c\rangle$ denotes a core and $|u\rangle$ an unoccupied valence state. Such intermediate states correspond to the initial state rule of x-ray absorption. Relaxation to the core hole may be accounted for by calculating the orbitals $|u\rangle$ not with ground state but with a screened core-hole potential, which would correspond to the final state rule of x-ray absorption. Putting together Eqs. (1) and (3) with the IPA states for $|0)$, $|m)$, and $|f)$ we obtain

$$I \sim -\frac{1}{\pi}\mathrm{Im}\int dx\, dx' M_k(x) g^+(x,x';\epsilon_v) M_k^*(x'), \tag{4}$$

where $g^+(x,x',\epsilon)$ is the position representation of the retarded Green's function G^+. Here, x is shorthand for $(\mathbf{r},\sigma)$. The matrix elements are given by

$$M_k(x) = \langle k|D|x\rangle + \sum_{uc}^{\epsilon_u>\epsilon_F} \frac{(\langle k,c| - \langle c,k|)V|x,u\rangle\langle u|D|c\rangle}{\hbar\omega + \epsilon_c - \epsilon_u - i\Gamma_c}. \tag{5}$$

We introduce the particle Green's function $g^p(z)$ defined as the single-particle Green's function for complex energy z and projected on the space of unoccupied states:

$$g^p(x,x';z) \equiv \sum_u^{\epsilon_u>\epsilon_F} \frac{\phi_u(x)\phi_u^*(x')}{z - \epsilon_u}.$$

With g^p, the sum over u can formally be omitted and we get

$$M_k(x) = \phi_k^*(x)D(x) + \sum_c \int dx'dx'' \frac{\phi_k^*(x)\phi_c^*(x') - \phi_k^*(x)\phi_c^*(x')}{|x - x'|} \times g^p(x',x'';\hbar\omega + \epsilon_c - i\Gamma_c)D(x'')\phi_c(x''). \quad (6)$$

Complex-valued single-particle Green's functions can be computed efficiently using multiple scattering theory.[51] This theoretical approach has been implemented in a real-space full multiple scattering method. Explicit formulas of the resonant cross section can be found in our previous paper.[38] Note, however, that the function g_p was not used, but the energy integration over ϵ_u in Eq. (5) was carried out numerically. The real-space multiple scattering code[38,52] is interfaced with self-consistent all-electron potentials obtained with the band-structure method linear muffin-tin orbital (LMTO). In this work on Fe(010), the atomic potentials were computed in the local spin density approximation for bulk ferromagnetic Fe. The calculated magnetic moment of $2.26\mu_B$ is in good agreement with experiment. The dipole and Auger matrix elements are calculated using scalar relativistic wave functions. From the latter, the spin-orbit-coupled $2p_{3/2}$ core states are built up. The much weaker spin-orbit coupling of the valence and continuum states has been neglected. For the optical transitions, the dipole approximation in the acceleration form is used[47] since the length form is not well defined for delocalized state. The theoretical spectra presented in the next sections include a Lorentzian broadening full width at half maximum (FWHM) of 0.2 eV.

II. RESULTS AND DISCUSSION

A. Spin-polarized MCD in angle-resolved RPES from a single Fe atom

First, we illustrate the resonance mechanism for the case of emission from one single Fe atom, and we discuss the energy dependence of the signal, the origin of spin-flip transitions, and spin polarization. The interstitial potential and the potential for the absorbing Fe site are the same as those used in the cluster calculations presented in the following paragraph. The difference is that all multiple scattering and thus all band-structure effects are absent. This allows us to focus on the intra-atomic origin of polarization and spin dependence of the resonant photocurrent. In Fig. 1, we show the spin- and angle-resolved direct valence band PES and RPES (spin-resolved ARPES and AR-RPES) cross section for left and right circular polarizations, for four photon energies across the L_3 edge and the corresponding constant initial state (CIS) spectra ($h\nu = 680.57$, 681.50, 683.83, 693.60 eV). The direction of the incoming beam is chosen to be collinear with the spin magnetic moment (parallel geometry) while the electron is emitted in a perpendicular direction.

Energy dependence. For the first photon energy, the decay channel is not yet open, thus only the direct valence band PES can take place [Fig. 1(a)]. The second photon energy is also in principle below threshold, but because of finite core-hole lifetime Γ_c, the onset of the opening of the resonant channel can occur at photon energies slightly below such nominal threshold [Fig. 1(b)]. For this photon energy, we observe a destructive interference between the direct and the resonant channels, i.e., the opening of the autoionization path decreases the total emission intensity. This corresponds to the dip region in the CIS spectrum. For the third photon energy, the intensity is strongly

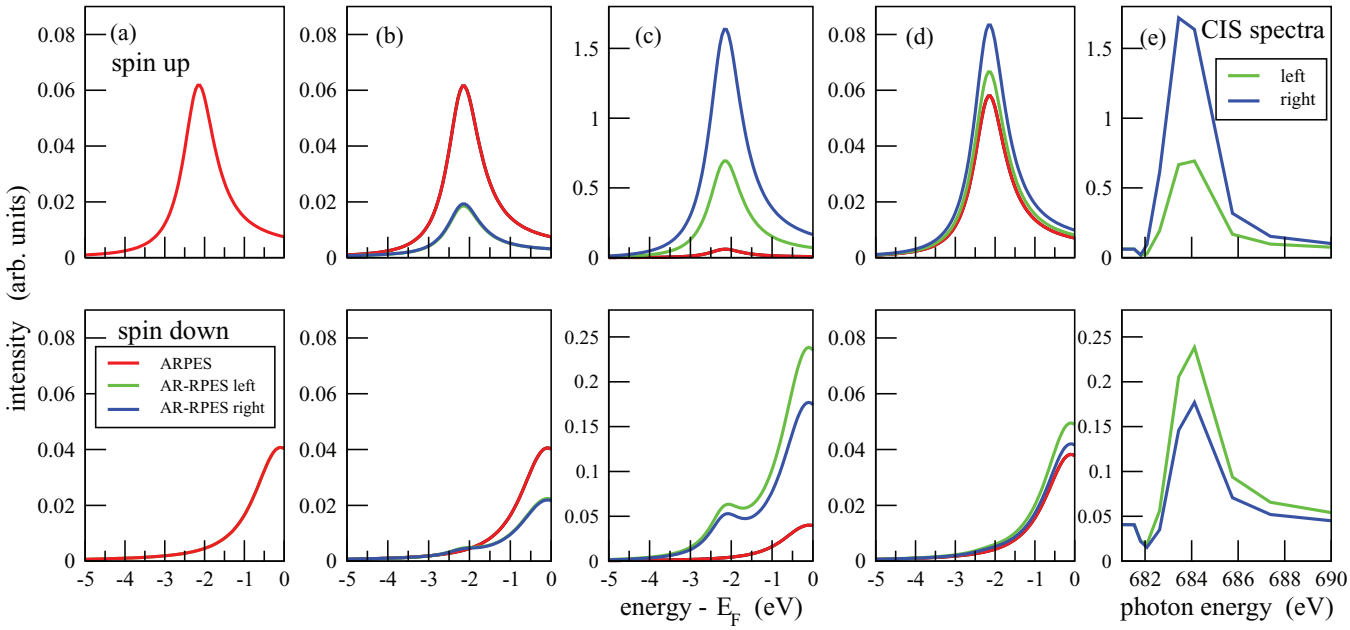

FIG. 1. (Color online) Spin- and angle-resolved direct valence band PES (ARPES) and RPES (AR-RPES) at the L_3 edge for one single Fe absorber in the single-atom limit, for light incidence along the magnetic moment (parallel geometry) and emission in a perpendicular direction. Left and right circular polarized light in green and blue. Direct PES process alone ("ARPES," red) for comparison. Photon energies are 680.57 (a), 681.50 (b), 683.83 (c), 693.60 eV (d). (e) Constant initial state (CIS) spectra at peak maxima ($E = -2.2/-0.2$ eV for spin up/down).

enhanced by the opening of the core-hole assisted channel [Fig. 1(c)], while far from the resonance the total intensity goes back to the one corresponding to the simple direct valence band PES process [Fig. 1(d)]. The CIS spectra [Fig. 1(e)] show a Fano profile typical of interference processes.

Spin-flip transitions. The direct valence band signal does not show circular dichroism. This is expected since for magnetic circular dichroism, spin-orbit (SO) coupling is necessary, but here such coupling is neglected in valence and continuum states. Circular dichroism in the angular distribution (CDAD) (Refs. 53–60) effects are also absent, as the geometrical setup is not chiral. The RPES signal, however, shows a large dichroism, which is maximum for the strongest enhancement of the signal and of opposite sign for the two spin channels. Since any band-structure effects are absent in this single-atom limit, the direct signal displays a single peak of Lorentzian shape typical for a d-wave potential scattering resonance and spin-up and -down peaks separated by the exchange splitting. At resonance, however, a new feature shows up in the spin-down channel corresponding to the energy of the peak of the spin-up channel (-2.2 eV). As there are (almost) no spin-down valence states at this energy, this peak in the spin-down photocurrent corresponds to spin-up initial states. This means that the spin of the photoelectron is opposite to the one of the final valence hole, and thus it is a spin-flip transition.

In a spin-flip process, the selection rule $\Delta S = 0$ is lifted since, due to considerable core SO coupling, spin is not a conserved quantity. The origin of such spin-flip transitions, both in resonant Auger and RIXS,[61–67] has always been at the center of a debate about whether they take place in the absorption step or in the core-hole decay. The spin-flip transitions observed here are a combined effect of spin-orbit coupling in the $2p_{3/2}$ core shell and exchange Coulomb decay. It is clear that direct Coulomb decay can not give rise to spin-flip transitions since the matrix element is $\langle k\sigma c\sigma'|V|v\sigma u\sigma'\rangle$ and so the photoelectron k and the valence hole v have necessarily the same spin. However, in exchange decay with matrix element $\langle c\sigma k\sigma'|V|v\sigma u\sigma'\rangle$, spin flip can occur for $\sigma = -\sigma'$. As the corresponding dipole transition matrix element is $\langle u\sigma'|D|c\sigma'\rangle$, the process also requires a spin flip of the core hole $|c\sigma'\rangle \rightarrow |c\sigma\rangle$. This is only possible when the core eigenstates have mixed spin character due to SO coupling, which is the case for the $2p_{3/2}$ $m_j = \pm\frac{1}{2}$ states.

Spin polarization. The peak intensity ratio between up and down spin is about 5:1 at maximum resonance [Fig. 1(c), averaging over the two light polarizations] while it is only about 3:2 off resonance [Fig. 1(a)]. So, the resonant process leads to a large enhancement of the valence band spin polarization. This can be understood as follows. Since the spin-up band is almost full, core-valence excitation can only happen for spin-down electrons. This means that the large majority of intermediate states are spin-down particle-hole excitations $|m) = a^+_{u\downarrow}a_{c\downarrow}|0)$. The autoionization decay of such intermediate states gives rise to both spin-up and -down electrons, but with very different transition probabilities. Spin-up photoelectrons $|k\uparrow\rangle$ can only be produced through direct Coulomb decay, whose matrix element is $V_D(\uparrow) = \langle k\uparrow c\downarrow|V|v\uparrow u\downarrow\rangle$. For spin-down electrons, the direct matrix element is $V_D(\downarrow) = \langle k\downarrow c\downarrow|V|v\downarrow u\downarrow\rangle$ and the corresponding transition probability is smaller by a factor $n(v\downarrow)/n(v\uparrow)$, where n are the ground-state occupation numbers. This is the same ratio as in the direct (nonresonant) photoemission process. So, if there were only direct Coulomb decay, resonant and nonresonant photoemission would have the same degree of spin polarization. The observed resonant enhancement of the spin polarization is due to the exchange decay. From intermediate states of the form $a^+_{u\downarrow}a_{c\downarrow}|0)$, exchange decay produces only spin-down electrons, with matrix element $V_X(\downarrow) = \langle c\downarrow k\downarrow|V|v\downarrow u\downarrow\rangle$. The total decay matrix element for spin-down photoelectrons is $V(\downarrow) = V_D(\downarrow) - V_X(\downarrow)$ [see Eq. (5)]. Now, $V_X(\downarrow)$ is comparable with $V_D(\downarrow)$ since the radial matrix elements are exactly the same when $|u\rangle$ and $|v\rangle$ are both $3d$ states. Thus, the exchange decay strongly reduces the spin-down transition amplitude with respect to the direct Coulomb decay alone. For spin-up photoelectrons, however, no such reduction occurs because $V_X(\uparrow) = 0$. This explains why the resonant process produces much more spin-up than spin-down electrons.

Note that already in our recent study on RPES from Cr (Ref. 38) we have argued that a core-valence excitation of one spin channel leads, through autoionization decay, to a majority of photoelectrons with the opposite spin. It is a crucial element in the explanation why the so-called mixed signal is nonzero even for a nonmagnetic ground state. This issue will be discussed here below, now for the case of a strong ferromagnet.

Interplay between dichroism and spin polarization. When using left $(+)$ or right $(-)$ circular polarized light and spin resolution $(\uparrow,\downarrow)$ of the photoelectrons, there are four independent spectra. We consider the following "fundamental" combinations:

$$\begin{aligned}
\text{tot} &= (+\uparrow) + (-\uparrow) + (+\downarrow) + (-\downarrow) \quad \text{(total)},\\
\text{dic} &= (+\uparrow) - (-\uparrow) + (+\downarrow) - (-\downarrow) \quad \text{(dichroic)}.\\
\text{spr} &= (+\uparrow) + (-\uparrow) - (+\downarrow) - (-\downarrow) \quad \text{(spin polarized)},\\
\text{mix} &= (+\uparrow) - (-\uparrow) - (+\downarrow) + (-\downarrow) \quad \text{(mixed)}.
\end{aligned}$$

In Fig. 2(a), we plot these fundamental spectra for a single Fe atom at maximum resonance. The setup is the same as in Fig. 1 with light incidence along the magnetization axis $(+z)$ and electron emission perpendicular to it $(+y)$.

The dichroic signal in Fig. 2(a) is large and negative, which is a direct consequence of the negative circular dichroism in x-ray absorption at the L_3 edge, which enters here as the excitation step in the resonant process. As expected from the direct valence band spectra in Fig. 1(a), the spin polarization changes sign between the majority spin peak at -2.2 eV and the minority spin peak around E_F. In resonant conditions, the majority spin peak is, however, much more enhanced than the minority peak (as discussed before) such that the spin-polarized spectra are dominated by the positive majority peak. The mixed signal is large and negative. It closely follows the dichroic signal along the majority peak, but stays negative at the minority peak contrary to the dichroic signal which becomes negligible around E_F. In Fig. 2(b), the magnetization direction is reversed ($M < 0$). As expected from their symmetry under time reversal, both dichroic and spin-polarized spectra change sign, while the mixed signal remains unchanged.[68] This confirms that the mixed signal analyzed in some earlier pioneering studies[22,23] is essentially

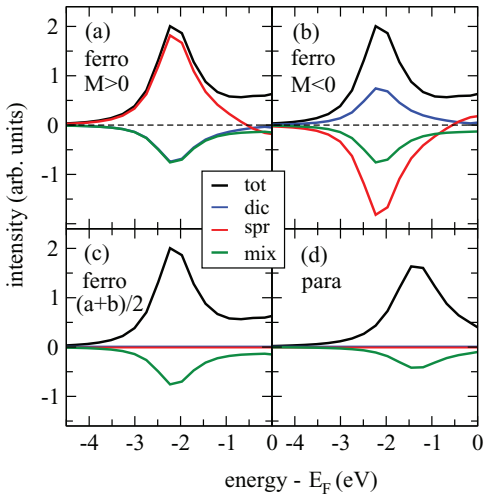

FIG. 2. (Color online) RPES at maximum resonance ($h\nu = 683.83$ eV) for a single Fe atom. Same geometry as in Fig. 1. Fundamental spectra total (tot), dichroic (dic), spin polarized (spr), and mixed (mix) for ferromagnetic (a)–(c) or Pauli paramagnetic (d) ground state.

independent of the orientation of the magnetic moments. In Fig. 2(c), we have plotted the average of the spectra in Figs. 2(a) and 2(b), meant as a simple model for a ferromagnet with vanishing macroscopic magnetization due to disordered moments or domain structure. Clearly, the spin-polarized and dichroic signals vanish, but the mixed signal does not, as found experimentally for Ni above the Curie temperature.[23] In Fig. 2(d), we show the fundamental spectra obtained for Fe with a nonmagnetic ground state, which would correspond to a Pauli paramagnetic system. As exchange splitting is absent, the spectrum consists of a single broad peak centered around -1.3 eV. For this nonmagnetic system and nonchiral setup, the dichroic and spin-polarized signals are obviously zero. However, the mixed signal is of the same sign and order of magnitude as that found in the ferromagnetic system [Figs. 2(a)–2(c)]. This shows that the mixed signal is mainly of nonmagnetic origin.

We have drawn the same conclusion previously in the case of Cr,[38] i.e., for a weak antiferromagnet. In that case, the mixed signal was found almost identical for the antiferromagnetic to the paramagnetic ground state.[38] In the present case of the Fe atom with large magnetic moment and exchange splitting, the mixed signal clearly changes both in position and amplitude when going from the magnetic [Figs. 2(a)–2(c)] to nonmagnetic ground state [Fig. 2(d)]. Qualitatively, the same changes are, however, observed for the total spectrum (tot), which means that the mixed signal does not yield more information about the magnetic state of the system than the total (isotropic) spectrum. Thus, our main conclusion from the Cr results is confirmed here for a ferromagnetic system with large moments: the mixed signal is not due to the presence of local magnetic moments, but rather reflects the spin-orbit coupling of the $2p_{3/2}$ shell, which is "transferred" to RPES through to the exchange process of the autoionization decay.[38]

B. Fe(010) RPES in parallel geometry and normal emission

We now move to the analysis of spin- and angle-resolved RPES from a Fe cluster. We start from the case of parallel geometry with normal emission for the outgoing electrons, and we discuss the energy dependence of the signal, the sensitivity to electronic states of different spin and orbital symmetry, and spin-flip transitions.

The Fe(010) surface is modeled with a semispherical cluster of 184 atoms and the magnetization is assumed in plane along ⟨001⟩. In Fig. 3(a), we show the comparison between the density of states (DOS) calculated by LMTO on bulk ferromagnetic Fe and our RSMS code for a central atom in the cluster. The agreement between the DOS by LMTO and the DOS for a central atom in the cluster is very good, showing that the bulk electronic properties are well described by the internal atoms of the cluster. Figures 3(c) and 3(d) show the band structure along the high-symmetry lines of the bcc Brillouin zone of bulk Fe [Fig. 3(b)], as calculated with the LMTO code.

The reference frame attached to the cluster is such that the z axis is defined by the magnetization direction, with the magnetic moment pointing along $+z$, the y axis is perpendicular to the surface, and the x axis is still lying on the surface. In the case of parallel geometry, the light incidence direction is along $+z$.

Energy dependence and MCD. In this geometry, the MCD in XAS is maximum since it essentially measures the projection of the magnetic moment onto the direction of the light incidence. In Fig. 4 we show the spin-resolved ARPES and AR-RPES intensities for the Fe(010) cluster for left and right circular polarization, again for four photon energies across the L_3 edge. In this geometrical setup, there is no source for additional purely geometric dichroism (CDAD) since all the relevant vectors are coplanar (and along high-symmetry directions) and hence there is no chirality induced solely by the experimental setup. We again observe a region of deconstructive interference [Fig. 4(b)] and then a strong enhancement for the third photon energy [Fig. 4(c)], which is different for the two spin channels. The massive enhancement of the signal observed here does not imply strong interference effects: an analysis of the different contributions in the amplitude reveals that, in our case, the enhancement is given essentially by the resonant excitation alone, as was also found in other cases.[8]

As compared to the single-atom spectra in Fig. 1, the cluster spectra show various new features due to electron scattering (discussed below in connection with the band structure of the system). However, in the geometry considered here, electron scattering does not seem to act as an additional source of dichroism since the sign and shape of the dichroic signal is essentially the same as in the single-atom case.

Sensitivity to orbital symmetry and spin-flip transitions. Let us now discuss the sensitivity of the ARPES and AR-RPES spectra to electronic states of different orbital symmetry. We shall first discuss the spin-up channel. The flat band along Γ-N-P-Γ around -1 eV in Fig. 3(d) gives rise to the strongest peak in the DOS as well as in the nonresonant photoelectron spectrum at normal emission. A projection of band states onto atomic orbitals (not shown) reveals that the flat band at -1 eV

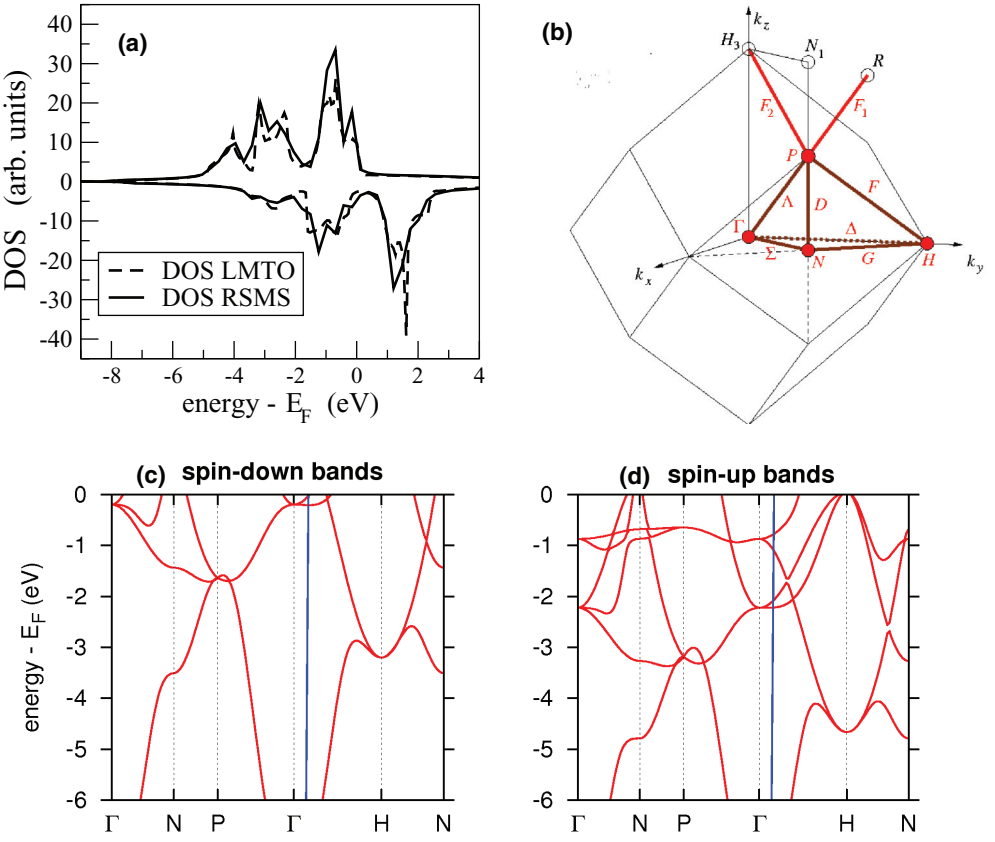

FIG. 3. (Color online) (a) DOS of bulk bcc Fe from periodic LMTO calculation compared with DOS on central atom in the cluster in RSMS calculation (positive/negative DOS for spin up/down); (b) bcc Brillouin zone; (c) spin-down and (d) spin-up bands from LMTO calculation (red) and final-state free-electron dispersion (blue).

is essentially of e_g character. The two states at the Γ point, at -0.9 and -2.2 eV, are of pure e_g and t_{2g} character, respectively. From $k_\parallel$ conservation it follows that for normal emission ($k_\parallel = 0$) the initial states lie on the Γ-H line. The peak positions of the spectrum can be found by plotting the final-state bands downshifted by the photon energy. The crossing points give the possible direct optical transitions in bulk Fe. Assuming free-electron dispersion, we have plotted the shifted final-state band for a photon energy of 683.8 eV and normal emission ($k_\parallel = 0$) as a blue line in Figs. 3(c) and 3(d). The crossing points are close to the Γ point because for $E(\text{initial}) = 0$, we have $k(\text{final}) = \frac{2\pi}{a}(0,0,6.16)$ and Γ (H) points are at even (odd) multiples of $\frac{2\pi}{a}(0,0,1)$. Note that since the slope of the final-state parabola is very large, a moderate change of the photon energy leads to only a small horizontal shift of the blue line, e.g., by 4% of the Γ-H distance for a photon energy change of 10 eV. It can be seen that the crossing points fit quite well the photoemission peaks around -0.8 and -2.0 eV, confirming the band-mapping interpretation of the valence band PES. Weak extra peaks (e.g., at -4.2 eV) may be due to umklapp processes which can lead to different crossing points on the Γ-H line.

It is interesting to note that in off-resonance conditions [Fig. 4(a)], the peak at -2.0 eV which corresponds to an initial state of t_{2g} character is much weaker than the e_g peak at -0.8 eV. This can essentially be understood from orbital selection rules. In a reference frame where the surface normal is chosen as the z axis, only $m_l = 0$ final states contribute to normal emission. From angular momentum recoupling coefficients and dipole selection rules it is then straightforward to show that for the dominating d to f transitions and the chosen light incidence, an initial e_g orbital leads to a three times larger normal emission intensity than a t_{2g} orbital. This argument, holds, however, only for the direct process, where the valence state symmetry together with the optical dipole selection rule essentially determines the angular distribution of the photoelectrons. For the autoionization process, however, the selection rules are more complex and involve also the symmetry of the core hole and excited state u. This might explain why at maximum resonance, where the autoionization process completely dominates, the t_{2g} peak at -2.0 eV is no longer suppressed, but is of comparable strength as the e_g peak at -0.8 eV [Fig. 4(c)].

Turning now to the spin-down channel, band-mapping analysis predicts a single normal emission peak close to E_F [crossing point in Fig. 3(c)]. The strongest peak is indeed observed at -0.2 eV. When going from the nonresonant [Fig. 4(a)] to the resonant spectrum [Fig. 4(c)], a new peak appears around -2.3 eV. This is clearly a spin-flip peak since its position and shape exactly match the largest peak of the resonant spin-up spectrum [Fig. 4(c), upper panel]. This shows that the spin-flip transitions, identified above in the single-atom case, must also be expected in AR-RPES from surfaces.

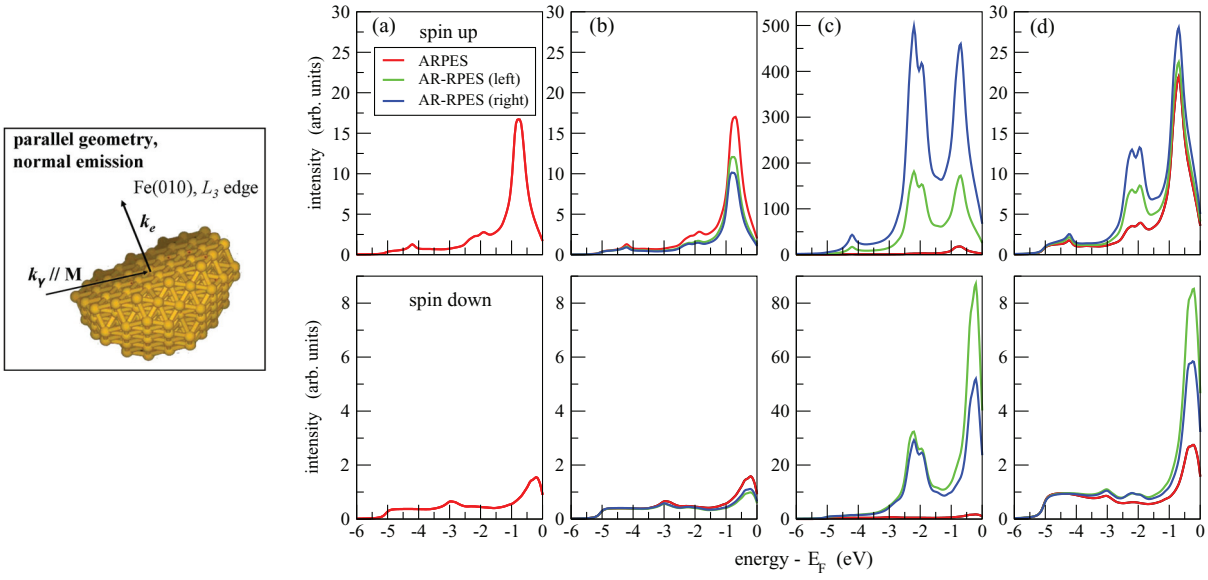

FIG. 4. (Color online) Spin- and angle-resolved RPES from the Fe(010) surface. Parallel geometry ($k_\gamma \parallel$ to M) and normal emission. Same photon energies as in Fig. 1: 680.57 (a), 681.50 (b), 683.83 (c), 693.60 eV (d).

C. Fe(010) RPES in perpendicular geometry: Normal and off-normal emission

We now move to the analysis of the often used *perpendicular* or *transverse geometry*, in which the signal allows us to probe directly the core-hole polarization[1] avoiding the contribution of the MCD due to the absorption step (which vanishes in this setup). Here, we consider RPES at maximum resonance and discuss circular dichroism and spin polarization of the photoelectrons as a function of emission direction. We analyze two types of perpendicular geometry: the first in which the photon beam direction lies on the surface and the second in which the beam is incoming perpendicular to the surface.

Perpendicular geometry, normal emission. In Fig. 5(a), we show the direct and resonant signals for the L_3 edge at the maximum of the resonance. k_γ lies on the surface, and in particular it is along $+x$. The magnetization is thus perpendicular to the scattering plane. The signal is spin polarized, as expected, but the amount of spin polarization, i.e., the ratio between the spin-up and -down intensity, is $\sim$3 here, and thus it is strongly different with respect to the case of parallel geometry (where it was $\sim$5). The dichroism, on the other hand, is zero. This is both because in perpendicular geometry MCD in the first absorption step is forbidden and because CDAD effects are absent (it is a completely orthogonal geometry, i.e., all three relevant vectors are orthogonal to each other and the emission is along a high-symmetry direction[53,69]). The symmetry between the two mirror conditions obtained by reversing the polarization of the light is indeed not broken when the magnetization is perpendicular to the plane of measurement.[70,71] The absence of dichroism in this geometry agrees with predictions from the atomic theory by Thole and van der Laan. Indeed, the geometrical factors $U(P,\epsilon,M)$ in Table I of Ref. 1 vanish when ϵ (which denotes the photoelectron direction) is perpendicular to M and P (which denotes k_γ).

Perpendicular geometry, off-normal emission. Most MCD experiments in both RPES and RIXS have been carried out in perpendicular geometry with x rays impinging along the surface normal. In Figs. 5(b) and 5(c), we show the spin-resolved ARPES and AR-RPES intensities for the maximum of the resonance at the L_3 edge in the case of such perpendicular geometry, for two different of-normal emission directions. We have analyzed both the cases in which the electron emission direction is coplanar with M and the photon direction k_γ [Fig. 5(b)] and the case in which it is not [Fig. 5(c)].

The coplanar case is similar to the one chosen in Refs. 6 and 71. The electron is emitted at polar angles (θ, ϕ)= (150°, 90°) in the Fe(010) reference frame where the surface normal is at (90°, 90°) and M at (0°, 0°). Since the magnetization, photon incidence, and electron emission are coplanar, there is no influence of CDAD in this setup [Fig. 5(b)] and thus only dichroism induced by the core-hole polarization is probed. The amount of spin polarization is strongly reduced with respect to the geometries considered before (as in the noncoplanar case discussed below), revealing that emission along non-high-symmetry directions strongly influences the degree of spin polarization in the photocurrent. However, still the spin-up channel is subjected to a relevant enhancement with respect to the spin-down channel; the origin of this has been already discussed in Sec. II A. Interestingly, in the coplanar emission case, we observe that, in our approach, the e_g peak at ~ -0.8 eV is suppressed for the spin-up channel, for both light helicities, suggesting that the orbital symmetry of the levels probed by the electron excited in the intermediate state can strongly influence the line shape. Furthermore, as the core-hole polarization is also determined by the population in the magnetic sublevels of the d band, other ground-state moments than the spin moment should also be taken into account, as they could play a role in determining the line shape at the resonance, by contributing in the enhancement or suppression of specific features.

In the noncoplanar case, the electron is emitted at (150°, 65°) [Fig. 5(d)] and one has the combined presence of both CDAD and dichroism induced by the core-hole polarization. Indeed, a nonzero (albeit weak) circular dichroism appears

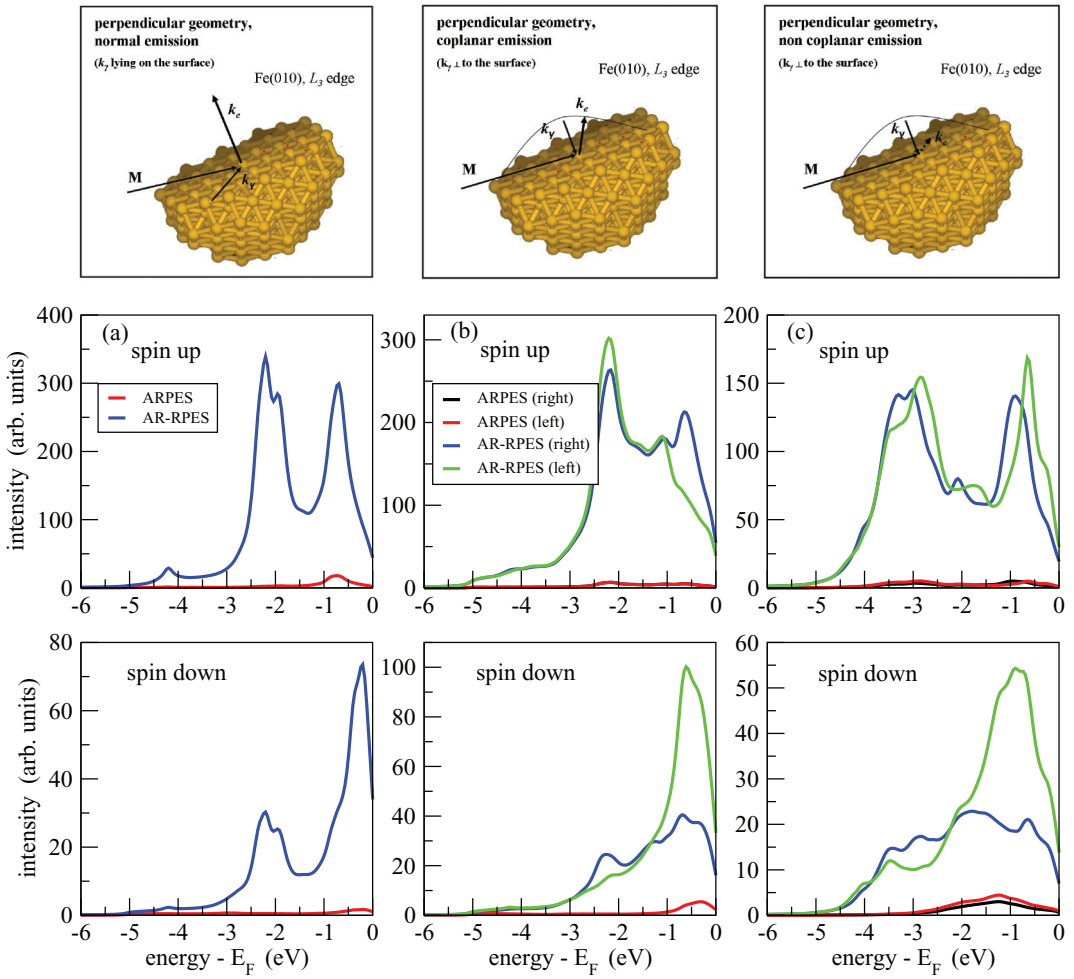

FIG. 5. (Color online) Spin-resolved ARPES and AR-RPES from the Fe(010) surface in perpendicular geometry (k_γ perpendicular to M) at maximum resonance ($h\nu = 683.83$ eV). (a) grazing incidence (along x), normal emission. (b) normal incidence (along y), off-normal emission at ($\theta = 150^\circ, \phi = 90^\circ$) polar angles, coplanar with M and k_γ. (c) normal incidence, off-normal emission at ($\theta = 150^\circ, \phi = 65^\circ$) non-coplanar with M and k_γ.

even in the direct signal because of purely geometric (CDAD) effects. Contrary to what was observed before in the case of parallel geometry and normal emission, the dichroism of the RPES signal in the two spin channels for the peak near E_F (of e_g and t_{2g} character for the spin-up and -down channels, respectively) is essentially of the same sign. Thus, in the case of a perpendicular geometry and off-normal emission directions, multiple scattering effects can even lead to a sign reversal of the spin-polarized MCD signal in correspondence to certain spectral features, as reported in previous works on both core and valence direct photoemission.[69,72–75] As a general trend, our results indicate that, when combining perpendicular geometry with off -normal emission directions, scattering effects do considerably influence the intensities, the dichroism, and photoelectron spin polarization.

D. Limitations of the method and possible future refinements

The present method is a fast and simple *ab initio* theory of angle-resolved RPES. As it is the first method of this kind, it contains several assumptions and approximations. The latter might limit its accuracy and range of applicability and they should therefore be overcome in the future. First, we have limited ourselves to the participator process. This obviously leads to problems for interpretation of experimental data if the (Raman-type) participator spectrum can not easily be separated from the (Auger-type) spectator spectrum. Second, the theory is formulated within the independent particle picture, which implies that it should give best results for weakly correlated systems. For Fe, relevant 3*d* electron correlations and a partial breakdown of the one-electron approach have been reported from measurements of unexpected magnetic dichroism in the transverse geometry in normal Auger spectroscopy[3] and from the description of real and imaginary parts of the quasiparticle self-energy.[76] Also, it is likely that the resonance enhancement of both the total and spin-polarized spectra are somewhat overestimated in the present approach because both the addition of the spectator channel and of many-body excitations would renormalize the single-particle participator response. For example, core-hole screening leads to an increase of the local valence charge and, generally, to a decrease of the valence spin polarization.[28,77] Finally, the same Fe bulk potential has

been used here for all atoms in the cluster, for simplicity. This may be easily improved by taking layer-dependent potentials from a self-consistent surface calculation. Thereby the change of local magnetic moment at the surface due to valence bands narrowing could be taken into account.[32,33,78] While this effect is rather small in Fe(010), it might be important for other compounds and less dense surfaces.

III. CONCLUSIONS

In summary, we have presented a first-principles method for valence band angle-resolved resonant photoelectron spectroscopy (AR-RPES) in a real-space multiple scattering approach. We have studied the spin-resolved ARPES and AR-RPES at the Fe $2p_{3/2}$-$3d$ resonance, focusing on circular dichroism and spin polarization of the photoelectrons emitted from a Fe(010) surface in various experimental geometries. Our results agree with qualitative predictions that can be gained from general symmetry considerations, atomic models, and the band structure of the system. While the AR-RPES spectra reflect the band structure in terms of peak positions, the relative peak intensities deviate considerably from nonresonant ARPES. Moveover, spin-flip transitions can lead to new peaks in the spin-resolved AR-RPES. The results on fundamental spectra confirm the conclusion drawn previously in the case of antiferromagnets[38] that the so-called mixed signal of combined circular polarized light and spin resolution is essentially unrelated to the existence of local magnetic moments. By comparing different geometries, we have also analyzed the influence of multiple scattering effects on dichroism and spin polarization for emission along high- and low-symmetry directions. At present, our method offers a fast and simple *ab initio* theory, which can provide useful information about local properties of low correlated systems, the estimation of the parameters of electron-electron and spin-spin interactions in the resonant decay, and can provide guidelines for future experiments.

ACKNOWLEDGMENT

F. Da Pieve acknowledges financial support from the VUB, Free University of Brussels, through the GOA77 project.

*fabiana.dapieve@gmail.com

[1] B. T. Thole, H. A. Dürr, and G. van der Laan, Phys. Rev. Lett. **74**, 2371 (1995).
[2] G. van der Laan and B. T. Thole, J. Phys.: Condens. Matter **7**, 9947 (1995); Phys. Rev. B **52**, 15355 (1995).
[3] H. A. Dürr, G. van der Laan, D. Spanke, F. U. Hillebrecht, and N. B. Brookes, J. Electron Spectrosc. Relat. Phenom. **93**, 233 (1998).
[4] F. Borgatti, G. Ghiringhelli, P. Ferriani, G. Ferrari, G. van der Laan, and C. M. Bertoni, Phys. Rev. B **69**, 134420 (2004).
[5] L. Braicovich, G. van der Laan, G. Ghiringhelli, A. Tagliaferri, M. A. van Veenendaal, N. B. Brookes, M. M. Chervinskii, C. Dallera, B. De Michelis, and H. A. Dürr, Phys. Rev. Lett. **82**, 1566 (1999).
[6] G. van der Laan, H. A. Dürr, and Mark Surman, J. Electron Spectrosc. Relat. Phenom. **78**, 213 (1996).
[7] G. van der Laan, B. T. Thole, H. Ogasawara, Y. Seino, and A. Kotani, Phys. Rev. B **46**, 7221 (1992).
[8] M. Magnuson, A. Nilsson, M. Weinelt, and N. Mårtensson, Phys. Rev. B **60**, 2436 (1999).
[9] M. W. Haverkort, Phys. Rev. Lett. **105**, 167404 (2010).
[10] L. Braicovich, G. Ghiringhelli, A. Tagliaferri, G. van der Laan, E. Annese, and N. B. Brookes, Phys. Rev. Lett. **95**, 267402 (2005).
[11] T. O. Mentes, F. Bondino, E. Magnano, M. Zangrando, K. Kuepper, V. R. Galakhov, Y. M. Mukovskii, M. Neumann, and F. Parmigiani, Phys. Rev. B **74**, 205409 (2006).
[12] P. A. Brühwiler, O. Karis, and N. Mårtensson, Rev. Mod. Phys. **74**, 703 (2002).
[13] M. H. Krisch, C. C. Kao, F. Sette, W. A. Caliebe, K. Hämäläinen, and J. B. Hastings, Phys. Rev. Lett. **74**, 4931 (1995).
[14] J. Danger, P. Le Fèvre, H. Magnan, D. Chandesris, S. Bourgeois, J. Jupille, T. Eickhoff, and W. Drube, Phys. Rev. Lett. **88**, 243001 (2002).
[15] G. Levy, R. Sutarto, D. Chevrier, T. Regier, R. Blyth, J. Geck, S. Wurmehl, L. Harnagea, H. Wadati, T. Mizokawa, I. S. Elfimov, A. Damascelli, and G. A. Sawatzky, Phys. Rev. Lett. **109**, 077001 (2012).
[16] P. Liu, Juan A. Colón Santana, Q. Dai, X. Wang, P. A. Dowben, and J. Tang, Phys. Rev. B **86**, 224408 (2012).
[17] K. Bapna, D. M. Phase, and R. J. Choudhary, J. Appl. Phys. **110**, 043910 (2011).
[18] T. Ohtsuki, A. Chainani, R. Eguchi, M. Matsunami, Y. Takata, M. Taguchi, Y. Nishino, K. Tamasaku, M. Yabashi, T. Ishikawa, M. Oura, Y. Senba, H. Ohashi, and S. Shin, Phys. Rev. Lett. **106**, 047602 (2011).
[19] A. Koitzsch, J. Ocker, M. Knupfer, M. C. Dekker, K. Dörr, B. Büchner, and P. Hoffmann, Phys. Rev. B **84**, 245121 (2011).
[20] P. Krüger, J. Jupille, S. Bourgeois, B. Domenichini, A. Verdini, L. Floreano, and A. Morgante, Phys. Rev. Lett. **108**, 126803 (2012).
[21] M. Morscher, F. Nolting, T. Brugger, and T. Greber, Phys. Rev. B **84**, 140406 (2011).
[22] L. H. Tjeng, B. Sinković, N. B. Brookes, J. B. Goedkoop, R. Hesper, E. Pellegrin, F. M. F. de Groot, S. Altieri, S. L. Hulbert, E. Shekel, and G.A. Sawatzky, Phys. Rev. Lett. **78**, 1126 (1997).
[23] B. Sinković, L. H. Tjeng, N. B. Brookes, J. B. Goedkoop, R. Hesper, E. Pellegrin, F. M. F. de Groot, S. Altieri, S. L. Hulbert, E. Shekel, and G. A. Sawatzky, Phys. Rev. Lett. **79**, 3510 (1997).
[24] U. Fano, Phys. Rev. **124**, 1866 (1961).
[25] N. Mårtensson, M. Weinelt, O. Karis, M. Magnuson, N. Wassdahl, A. Nilsson, J. Stöhr, and M. Samant, Appl. Phys. A **65**, 159 (1997).
[26] C. O. Almbladh and L. Hedin, in *Handbook on Synchrotron Radiation*, edited by E. E. Koch (North-Holland, Amsterdam, New York, 1983), Vol. 1B, p. 607.
[27] M. Weinelt, A. Nilsson, M. Magnuson, T. Wiell, N. Wassdahl, O. Karis, A. Fohlisch, N. Mårtensson, J. Stöhr, and M. Samant, Phys. Rev. Lett. **78**, 967 (1997).

[28]A. Chassé, H. A. Dürr, G. van der Laan, Yu. Kucherenko, and A. N. Yaresko, Phys. Rev. B **68**, 214402 (2003).
[29]B. Sinković, E. Shekel, and S. L. Hulbert, Phys. Rev. B **52**, R15703 (1995).
[30]A. Kotani, J. Appl. Phys. **57**, 3632 (1985).
[31]R. Gotter, G. Fratesi, R. A. Bartynski, F. Da Pieve, F. Offi, A. Ruocco, S. Ugenti, M. I. Trioni, G. P. Brivio, and G. Stefani, Phys. Rev. Lett. **109**, 126401 (2012).
[32]F. Sirotti and G. Rossi, Phys. Rev. B **49**, 15682 (1994).
[33]B. T. Thole and G. van der Laan, Phys. Rev. Lett. **67**, 3306 (1991); Phys. Rev. B **44**, 12424 (1991).
[34]F. U. Hillebrecht, Ch. Roth, H. B. Rose, M. Finazzi, and L. Braicovich, Phys. Rev. B **51**, 9333 (1995).
[35]F. U. Hillebrecht, Ch. Roth, H. B. Rose, W. G. Park, E. Kisker, and N. A. Cherepkov, Phys. Rev. B **53**, 12182 (1996).
[36]J. J. Kas, J. J. Rehr, J. A. Soininen, and P. Glatzel, Phys. Rev. B **83**, 235114 (2011).
[37]F. M. F. de Groot, J. Electron Spectrosc. Relat. Phenom. **92**, 207 (1998).
[38]F. Da Pieve and P. Krüger, Phys. Rev. Lett. **110**, 127401 (2013).
[39]L. C. Davis and L. A. Feldkamp, Phys. Rev. B **23**, 6239 (1981).
[40]T. Åberg and G. Howat, in *Corpuscles, and Radiation in Matter I*, edited by S. Flugge and W. Mehlorn, Vol. 31 of Handuch der Physik (Springer, Berlin, 1982), p. 469.
[41]T. Aberg, Phys. Scr. **21**, 495 (1980).
[42]F. Gel'mukhanov and H. Ågren, Phys. Rep. **312**, 87 (1999).
[43]K. Cho and Y. Miyamoto, Surf. Sci. Lett. **192**, L835 (1987).
[44]C. Janowitz, R. Manzke, M. Skibowski, Y. Takeda, Y. Miyamoto, and K. Cho, Surf. Sci. Lett. **275**, L669 (1992).
[45]A. Tanaka and T. Jo, J. Phys. Soc. Jpn. **63**, 2788 (1994).
[46]F. Da Pieve, D. Sébilleau, S. Di Matteo, R. Gunnella, R. Gotter, A. Ruocco, G. Stefani, and C. R. Natoli, Phys. Rev. B **78**, 035122 (2008).
[47]J. B. Pendry, Surf. Sci. **57**, 679 (1976).
[48]J. Braun, Rep. Prog. Phys. **59**, 1267 (1996).
[49]A. W. Kay, F. J. Garcia de Abajo, S.-H. Yang, E. Arenholz, B. S. Mun, N. Mannella, Z. Hussain, M. A. Van Hove, and C. S. Fadley, Phys. Rev. B **63**, 115119 (2001).
[50]A. Kay, E. Arenholz, S. Mun, F. J. Garcia de Abajo, C. S. Fadley, R. Denecke, Z. Hussain, and M. A. Van Hove, Science **281**, 679 (1998).
[51]D. Sébilleau, R. Gunnella, Z.-Y. Wu, S. Di Matteo, and C. R. Natoli, J. Phys.: Condens. Matter **18**, R175 (2006).
[52]P. Krüger, F. Da Pieve, and J. Osterwalder, Phys. Rev. B **83**, 115437 (2011).
[53]G. van der Laan, J. Magn. Magn. Mater. **148**, 53 (1995).
[54]C. Westphal, F. Fegel, J. Bansmann, M. Getzlaff, G. Schönhense, J. A. Stephens, and V. McKoy, Phys. Rev. B **50**, 17534 (1994).
[55]G. Fecher, Eruophys. Lett. **29**, 605 (1995).
[56]C. Westphal, J. Bansmann, M. Getzlaff, and G. Schönhense, Phys. Rev. Lett. **63**, 151 (1989).
[57]G. Schönhense, Phys. Scr., T **31**, 255 (1990).
[58]B. Ritchie, Phys. Rev. A **12**, 567 (1975).
[59]R. Parzynski, Act. Phys. Pol., A **57**, 49 (1980).
[60]N. A. Cherepkov, Chem. Phys. Lett. **87**, 344 (1982); Adv. At. Mol. Phys. **19**, 395 (1983).
[61]C. Laubschat, E. Weschke, G. Kalkowski, and G. Kaindl, Phys. Scr. **41**, 124 (1990).
[62]T. Kachel, W. Gudat, C. Carbone, E. Vescovo, S. Blügel, U. Alkemper, and W. Eberhardt, Phys. Rev. B **46**, 12888 (1992).
[63]J.-J. Gallet, J.-M. Mariot, C. F. Hague, F. Sirotti, M. Nakazawa, H. Ogasawara, and A. Kotani, Phys. Rev. B **54**, R14238 (1996).
[64]C. Dallera, L. Braicovich, G. Ghiringhelli, M. A. van Veenendaal, J. B. Goedkoop, and N. B. Brookes, Phys. Rev. B **56**, 1279 (1997).
[65]S. G. Chiuzbaian, G. Ghiringhelli, C. Dallera, M. Grioni, P. Amann, X. Wang, L. Braicovich, and L. Patthey, Phys. Rev. Lett. **95**, 197402 (2005).
[66]L. Braicovich, C. Dallera, G. Ghiringhelli, N. B. Brookes, J. B. Goedkoop, and M. A. van Veenendaal, Phys. Rev. B **55**, R15989 (1997).
[67]F. Gerken, J. Barth, and C. Kunz, Phys. Rev. Lett. **47**, 993 (1981).
[68]G. van der Laan, Phys. Rev. Lett. **81**, 733 (1998).
[69]J. Henk, A. M. N. Niklasson, and B. Johansson, Phys. Rev. B **59**, 13986 (1999).
[70]W. Kuch and C. M. Schneider, Rep. Prog. Phys. **64**, 147 (2001).
[71]M. Finazzi, G. Ghiringhelli, O. Tjernberg, and N. B. Brookes, J. Phys.: Condens. Matter **12**, 2123 (2000).
[72]G. D. Waddill, J. G. Tobin, X. Guo, and S. Y. Tong, Phys. Rev. B **50**, 6774 (1994).
[73]A. Chassé, J. Phys.: Condens. Matter **11**, 6475 (1999).
[74]C. M. Schneider, D. Venus, and J. Kirschner, Phys. Rev. B **45**, 5041 (1992).
[75]D. Venus, L. Baumgarten, C. M. Schneider, C. Boeglin, and J. Kirschner, J. Phys.: Condens. Matter **5**, 1239 (1993).
[76]J. Sánchez-Barriga, J. Braun, J. Minár, I. Di Marco, A. Varykhalov, O. Rader, V. Boni, V. Bellini, F. Manghi, H. Ebert, M. I. Katsnelson, A. I. Lichtenstein, O. Eriksson, W. Eberhardt, H. A. Dürr, and J. Fink, Phys. Rev. B **85**, 205109 (2012).
[77]Yu. Kucherenko, B. Sinković, E. Shekel, P. Rennert, and S. Hulbert, Phys. Rev. B **62**, 5733 (2000).
[78]B. Sinković, E. Shekel, and S. L. Hulbert, Phys. Rev. B **52**, R8696 (1995).